SUPPORTING INFORMATION

Peak P-T conditions in the deepest rocks from the Western Alps: The Pinerolo Unit (Dora-Maira Massif)

Author names

Paola Manzotti[1*], Federica Schiavi[2], Francesca Piccoli[3], William Westin[1,4], Michel Ballèvre[5]

Affiliations:

[1] Department of Geological Sciences, Stockholm University, 106 91 Stockholm, Sweden

[2] Université Clermont Auvergne, CNRS, IRD, OPGC, Laboratoire Magmas et Volcans, 63000 Clermont-Ferrand, France

[3] Institute of Geological Sciences, University of Bern, Bern CH-3012, Switzerland

[4] Bergab – Berggeologiska undersökningar AB, Stockholm, Sweden

[5] Geosciences Rennes-UMR 6118, University of Rennes, F35000, Rennes, France

Corresponding author

*Correspondence: paola.manzotti@geo.su.se Tel. +46 (0)8 16 4745, ORCID: 0000-0002-6945-9878

Laboratory		
Microsonde Ouest, Brest (France)		
Instrument		
Cameca SX100 equipped with 5 WDS spectrometers		
Operating conditions for spot analyses		
15 kV accelerating voltage, 20 nA beam current, spot size = 1 μm. ϕ(ρZ) matrix correction was applied based on Pouchou and Pichoir (1985)		
Analysed mineral		
garnet, white mica, chlorite, biotite, rutile, ilmenite, titanite		
Standard	**Counting time (peak)**	**Counting time (background)**
albite: Na, Si	10	5
orthoclase: K	10	5
corundum: Al	10	5
wollastonite: Ca	10	5
forsterite: Mg	10	5
$MnTiO_3$: Mn, Ti	30	15
andradite: Fe	10	5
Cr_2O_3: Cr	10	5
NiO: Ni	10	5
Operating conditions for muscovite X-ray maps		
15 kV accelerating voltage, 20 nA beam current, 1 μm beam, 0.15 s, 2 μm step		

Table S1 Operating conditions for microprobe analyses

Mineral abbreviations	
ab	albite
alm	almandine
bi	biotite
chl	chlorite
ctd	chloritoid
ep	epidote
g	garnet
gl	glaucophane
grs	grossular
ilm	ilmenite
jd	jadeite
law	lawsonite
mu	muscovite
olg	oligoclase
pa	paragonite
pl	plagioclase
prp	pyrope
q	quartz
ru	rutile
spss	spessartine
sph	titanite

Other symbols (mole/atomic proportions)	
X_{Mg}	Mg/(Fe + Mg)
X_{Na}	Na/(Na+K)
alm	$Fe^{2+}/(Fe^{2+} + Mg + Ca + Mn)$
spss	$Mn/(Fe^{2+} + Mg + Ca + Mn)$
prp	$Mg/(Fe^{2+} + Mg + Ca + Mn)$
grs	$Ca/(Fe^{2+} + Mg + Ca + Mn)$
wt%	weight per cent
mol%	mole per cent
vol.%	volume per cent

Table S2 Mineral abbreviations and other symbols used in this study

Mineral	g	g	g	g	g	g	mu	mu	mu	mu	mu	mu	mu	mu	chl	chl	ru	ilm
Zone	rim	rim	rim	core	core	core	S_1 core (area 1)	S_1 rim (area 1)	S_1 core (area 2)	S_1 rim (area 2)	S_2 core (area 3)	S_2 rim (area 3)	S_2 core (area 8)	S_2 rim (area 5)	matrix	matrix	in g core	matrix
Analysis	6	68	71	36	43	25	153	152	137	130	66	12	38	97	30	78	77	47
SiO_2	36.80	36.94	36.86	36.48	36.65	36.74	51.66	46.88	51.29	46.59	51.50	46.42	51.68	47.09	24.86	24.74	0.09	0.09
TiO_2	0.02	0.06	0.04	0.04	0.05	<0.01	0.17	0.20	0.17	0.21	0.12	0.19	0.17	0.27	<0.01	0.06	99.21	53.00
Cr_2O_3	<0.01	<0.01	<0.01	<0.01	<0.01	<0.01	<0.01	<0.01	<0.01	<0.01	<0.01	<0.01	<0.01	0.01	<0.01	<0.01	0.00	<0.01
NiO	0.04	0.03	<0.01	<0.01	0.03	0.04	0.03	<0.01	0.07	0.01	<0.01	0.03	<0.01	0.02	0.03	0.04	0.00	<0.01
Al_2O_3	21.16	21.10	21.18	21.43	20.95	21.10	27.73	34.87	27.46	35.39	27.03	35.77	27.97	34.95	21.81	22.46	0.05	0.03
FeO	32.17	31.55	31.94	28.88	29.97	30.70	3.26	1.74	3.20	1.48	3.31	1.38	3.01	1.50	29.47	28.86	1.19	45.78
MnO	2.35	2.30	2.39	5.52	5.06	4.79	<0.01	<0.01	0.01	<0.01	<0.01	<0.01	<0.01	<0.01	0.08	0.08	0.10	0.54
MgO	1.13	1.21	0.93	0.81	0.87	0.89	2.63	0.76	2.74	0.68	2.82	0.64	2.65	0.85	11.81	11.88	0.01	0.21
CaO	6.94	7.15	7.35	6.67	6.34	6.29	<0.01	0.03	<0.01	<0.01	0.01	0.03	<0.01	0.03	0.01	0.06	<0.01	<0.01
Na_2O	<0.01	0.05	0.06	0.17	0.09	0.09	0.40	0.65	0.41	0.98	0.28	1.36	0.33	1.13	0.01	<0.01	<0.01	<0.01
K_2O	<0.01	<0.01	<0.01	<0.01	<0.01	<0.01	9.98	10.16	9.97	9.99	10.33	9.43	9.93	9.38	0.01	0.04	<0.01	<0.01
Total	100.61	100.39	100.75	100.00	100.01	100.64	95.86	95.29	95.32	95.33	95.40	95.25	95.74	95.23	88.09	88.22	100.65	99.53
Oxygen-equivalents	12	12	12	12	12	12	11	11	11	11	11	11	11	11	14	14	2	3
Si	2.95	2.96	2.95	2.94	2.96	2.95	3.42	3.12	3.42	3.09	3.44	3.08	3.42	3.12	2.66	2.64	0.00	0.02
Ti	0.00	0.00	0.00	0.00	0.00	0.00	0.01	0.01	0.01	0.01	0.01	0.01	0.01	0.01	0.00	0.00	1.98	1.00
Cr	0.00	0.00	0.00	0.00	0.00	0.00	0.00	0.00	0.00	0.00	0.00	0.00	0.00	0.00	0.00	0.00	0.00	0.00
Ni	0.00	0.00	0.00	0.00	0.00	0.00	0.00	0.00	0.00	0.00	0.00	0.00	0.00	0.00	0.00	0.00	0.00	0.00
Al	2.00	1.99	2.00	2.03	1.99	2.00	2.17	2.73	2.16	2.77	2.13	2.80	2.18	2.73	2.75	2.82	0.00	0.00
Fe^{3+}	0.10	0.08	0.11	0.11	0.09	0.12	0.00	0.00	0.00	0.00	0.00	0.00	0.00	0.00	0.00	0.00	0.00	0.00
Fe^{2+}	2.06	2.03	2.03	1.84	1.93	1.95	0.18	0.10	0.18	0.08	0.18	0.08	0.17	0.08	2.64	2.57	0.01	0.96
Mn	0.16	0.16	0.16	0.38	0.35	0.33	0.00	0.00	0.00	0.00	0.00	0.00	0.00	0.00	0.01	0.01	0.00	0.01
Mg	0.13	0.10	0.11	0.10	0.11	0.11	0.26	0.08	0.27	0.07	0.28	0.06	0.26	0.08	1.89	1.89	0.00	0.01
Ca	0.60	0.61	0.63	0.58	0.55	0.54	0.00	0.00	0.00	0.00	0.00	0.00	0.00	0.00	0.00	0.01	0.00	0.00
Na	0.00	0.01	0.01	0.00	0.01	0.00	0.05	0.08	0.05	0.13	0.04	0.18	0.04	0.15	0.00	0.00	0.00	0.00
K	0.00	0.00	0.00	0.00	0.00	0.00	0.84	0.86	0.85	0.85	0.88	0.80	0.84	0.79	0.00	0.01	0.00	0.00
Total	8.00	8.00	8.00	7.98	7.99	8.00	6.93	6.98	6.94	7.00	6.96	7.01	6.92	6.96	9.95	9.95	2.00	2.00
X_{Mg}	0.06	0.05	0.05	0.05	0.05	0.05	0.59	0.44	0.60	0.47	0.61	0.43	0.60	0.50	0.42	0.42		
alm	70	70	69	63	66	67												
prp	4	3	4	3	4	4												
grs	20	21	22	20	19	18												
spss	5	6	5	13	12	11												

Table S3 Representative mineral analyses and formulas from the chlorite-rich schist Pi14. Garnet analyses are selected along the A-B profile indicated in Figure 5h

Mineral	g	g	g	g	g	g	mu	mu	mu	mu	mu	mu	mu	mu	mu	mu	pa	bi	bi	ru	ilm	ilm	sph
Zone	rim	rim	mantle	mantle	core	core	S_2 core (area 1)	S_2 core (area 1)	S_2 rim (area 1)	S_2 rim (area 1)	S_2 core (area 2)	S_2 core (area 2)	pressure shadow	pressure shadow	inclusion in ab	inclusion in sph	inclusion in sph	replacing chl	replacing chl	inclusion in g core	inclusion in ab	replacing sph	matrix
Analysis	42	43	35	5	29	21	84	98	90	96	67	62	51	60	58	16	29	45	53	23	111	44	25
SiO_2	37.47	37.99	37.58	37.37	37.53	37.51	50.11	50.76	47.12	46.59	50.46	50.81	46.81	46.49	49.81	50.51	47.20	35.97	36.43	0.08	0.05	0.10	30.62
TiO_2	0.07	0.13	0.16	0.13	0.10	0.18	0.30	0.23	0.20	0.42	0.24	0.42	0.23	0.28	0.41	0.53	0.80	1.50	1.61	99.15	53.20	54.15	37.88
Cr_2O_3	<0.01	0.03	0.03	0.05	0.04	0.02	0.01	0.04	0.01	0.14	0.08	0.05	0.08	0.09	0.12	0.09	0.04	0.07	0.08	<0.01	0.05	0.03	<0.01
NiO	0.02	<0.01	<0.01	0.02	0.06	<0.01	0.01	0.10	<0.01	0.03	0.02	0.08	0.05	<0.01	<0.01	0.05	0.06	<0.01	<0.01	<0.01	<0.01	<0.01	<0.01
Al_2O_3	21.12	21.25	21.04	21.23	21.28	21.23	28.50	28.03	35.90	34.11	28.49	28.73	36.37	35.75	29.65	28.24	39.90	18.72	19.02	0.06	0.04	0.03	1.85
FeO	29.15	28.65	30.75	30.99	30.90	30.89	3.56	3.55	1.52	1.70	3.20	2.87	1.37	1.43	2.57	3.48	0.31	18.49	18.12	1.27	45.84	42.62	0.15
MnO	2.46	2.61	1.52	1.58	2.09	2.38	0.05	<0.01	<0.01	<0.01	<0.01	0.05	<0.01	<0.01	0.01	0.03	0.02	0.13	0.07	0.06	0.21	2.15	0.07
MgO	0.76	0.76	0.66	0.67	0.66	0.70	2.68	2.64	1.07	1.27	2.73	2.83	0.90	0.93	2.62	2.84	0.08	9.78	9.60	0.02	0.19	0.06	<0.01
CaO	10.15	10.31	9.40	8.94	8.79	8.44	0.02	<0.01	0.01	<0.01	0.01	<0.01	<0.01	0.01	0.02	0.13	0.40	0.03	0.03	<0.01	<0.01	<0.01	29.20
Na_2O	0.04	0.03	0.05	0.03	0.01	0.05	0.30	0.26	0.80	0.60	0.36	0.30	1.16	0.95	0.36	0.28	7.02	0.08	0.09	<0.01	<0.01	<0.01	<0.01
K_2O	<0.01	<0.01	0.01	0.01	<0.01	<0.01	10.58	10.96	10.17	10.37	10.79	10.50	9.50	10.25	10.77	10.22	0.37	9.53	9.13	<0.01	<0.01	<0.01	<0.01
Total	101.24	101.74	101.20	101.02	101.46	101.40	96.12	96.59	96.80	95.21	96.37	96.64	96.46	96.17	96.34	96.39	96.19	94.28	94.17	100.63	99.58	99.13	99.76
Oxygen-equivalents	12	12	12	12	12	12	11	11	11	11	11	11	11	11	11	11	11	12	12	2	3	3	5
Si	2.97	2.99	2.99	2.98	2.98	2.98	3.34	3.37	3.08	3.11	3.35	3.35	3.06	3.07	3.30	3.35	2.98	2.75	2.77	0.00	0.00	0.00	1.00
Ti	0.00	0.01	0.01	0.01	0.01	0.01	0.02	0.01	0.01	0.02	0.01	0.02	0.01	0.01	0.02	0.03	0.04	0.09	0.09	0.99	1.01	1.02	0.93
Cr	0.00	0.00	0.00	0.00	0.00	0.00	0.00	0.00	0.00	0.01	0.00	0.00	0.00	0.00	0.01	0.00	0.00	0.00	0.00	0.00	0.00	0.00	0.00
Ni	0.00	0.00	0.00	0.00	0.00	0.00	0.00	0.01	0.00	0.00	0.00	0.00	0.00	0.00	0.00	0.00	0.00	0.00	0.00	0.00	0.00	0.00	0.00
Al	1.97	1.97	1.97	1.99	1.99	1.99	2.24	2.19	2.77	2.68	2.23	2.23	2.81	2.78	2.31	2.21	2.97	1.69	1.71	0.00	0.00	0.00	0.07
Fe^{3+}	0.09	0.03	0.05	0.04	0.04	0.04	0.00	0.00	0.00	0.00	0.00	0.00	0.00	0.00	0.00	0.00	0.00	0.00	0.00	0.00	0.00	0.00	0.00
Fe^{2+}	1.84	1.86	2.00	2.02	2.01	2.01	0.20	0.20	0.08	0.09	0.18	0.16	0.07	0.08	0.14	0.19	0.02	1.18	1.15	0.01	0.97	0.90	0.00
Mn	0.17	0.17	0.10	0.11	0.14	0.16	0.00	0.00	0.00	0.00	0.00	0.00	0.00	0.00	0.00	0.00	0.00	0.01	0.00	0.00	0.00	0.05	0.00
Mg	0.09	0.09	0.08	0.08	0.08	0.08	0.27	0.26	0.10	0.13	0.27	0.28	0.09	0.09	0.26	0.28	0.01	1.12	1.09	0.00	0.01	0.00	0.00
Ca	0.86	0.87	0.80	0.76	0.75	0.72	0.00	0.00	0.00	0.00	0.00	0.00	0.00	0.00	0.00	0.01	0.03	0.00	0.00	0.00	0.00	0.00	1.03
Na	0.01	0.00	0.01	0.00	0.00	0.01	0.04	0.03	0.10	0.08	0.05	0.04	0.15	0.12	0.05	0.04	0.86	0.01	0.01	0.00	0.00	0.00	0.00
K	0.00	0.00	0.00	0.00	0.00	0.00	0.90	0.93	0.85	0.88	0.91	0.88	0.79	0.86	0.91	0.86	0.03	0.93	0.89	0.00	0.00	0.00	0.00
Total	8.00	7.99	8.01	7.99	8.00	8.00	7.01	7.00	6.99	7.00	7.00	6.96	6.98	7.01	7.00	6.97	6.94	7.78	7.71	1.00	1.99	1.97	3.03
X_{Mg}	0.05	0.05	0.04	0.04	0.04	0.04	0.57	0.57	0.56	0.59	0.60	0.64	0.56	0.53	0.65	0.60	0.33	0.49	0.49				
alm	62	62	67	68	67	68																	
prp	3	3	3	3	3	3																	
grs	29	29	27	26	25	24																	
spss	6	6	3	4	5	5																	

Table S4 Representative mineral analyses and formulas from the albite micaschist Pi15. Garnet analyses are selected along the A-B profile indicated in Figure 7f

Unit	Sample	SiO_2	Al_2O_3	Fe_2O_3	MnO	MgO	CaO	Na_2O	K_2O	TiO_2	P_2O_5
Pinerolo Unit	Pi14 chl-rich schist	63.79	19.14	7.37	0.11	2.30	0.45	0.30	5.11	1.32	0.12
	Pi15 ab micaschist	72.95	15.01	4.28	0.07	1.50	0.46	1.04	3.80	0.85	0.06

Table S5 Whole-rock compositions for the studied samples (wt%)

Software		
Theriak-Domino (de Capitani and Brown 1987; de Capitani and Petrakakis 2010)		
Thermodynamic dataset		
Holland and Powell (1998, 2011) version ds62		
Solution models (minerals)		
	Mineral	**Solution model**
Orthosilicates	Garnet	Holland and Powell 2011; White et al. 2014a, 2014b
	Kyanite	pure
	Chloritoid	Holland and Powell 2011; White et al. 2014a, 2014b
	Staurolite	Holland and Powell 2011; White et al. 2014a, 2014b
Cyclosilicates	Cordierite	Holland and Powell 2011; White et al. 2014a, 2014b
Disilicates	Epidote	Holland and Powell 2011
	Lawsonite	pure
Chain silicates	Clinopyroxene	Green et al. 2016
	Amphibole	Green et al. 2016
Sheet silicates	White mica	White et al. 2014a, 2014b
	Biotite	White et al. 2014a, 2014b
	Chlorite	White et al. 2014a, 2014b
Framework silicates	Plagioclase	Holland et al. 2022
	Quartz/Coesite	pure
Oxydes	Magnetite	Holland and Powell 2011; Powell et al. 2014
	Rutile	pure
	Ilmenite	Holland and Powell 2011; White et al. 2014a, 2014b
Solution models (fluid)		
	H_2O	pure

Table S6 Phases and activity composition models considered in the thermodynamic calculations

Unit	Sample	Lithology	GPS Lat Long coordinates	Mineral assemblage	n	R2	T (°C)	SD	Confidence
Pinerolo	Pi3	chl micaschist	N44° 57' 30.54'' E7° 13' 36.29''	q 25 %, wm 25%, chl 20%, g 10%, gph 10%, ilm 5%, ab 5%, ru <5%	22	0.09-0.36	531	21	9
	Pi4	ab micaschist	N44° 57' 3.02'' E7° 9' 56.45''	q 40%, ab 25%, wm 15%, chl 15%, g 5%, bi<5%	16	0.1-0.29	551	23	12
	Pi5	ab micaschist	N44° 56' 25.52'' E7° 9' 18.17''	q 40%, ab 25%, wm 15%, g 10%, chl 5%, gph <5%, bi <5%	21	0.14-0.40	538	22	10
	Pi19	chl micaschist	N44° 57' 20.37'' E7° 8' 43.42''	q 40%, wm 25%, chl 15%, ab 15%, bi 5%, gph < 5%, g <5%	22	0.14-0.35	539	21	9
	Pi14	chl-rich schist	44°57'44.79"N 7°10'17.75"E	q 40%, wm 35%, chl 15%, g <5%, ilm <5%, gph 1%, ru <5%, ab <5%, ep <5%	24	0.27-0.38	496	16	6
	Pi25	ab micaschist	44°59'05.59"N 7°06'43.95"E	q 25%, wm 30%, chl 15%, ab 15%, g 5%, gph 5%, ep <5%, ru <5%, ilm <5%, tur <5%	23	0.17-0.41	500	27	11
Chasteiran	CH47	ctd micaschist	N44° 56' 57.93'' E7° 08' 14.48''	mu 35%, q 20%, chl 15%, ctd 5%, ilm 10%, gph 10%, ab 5%,	20	0.19-0.39	488	17	7
	CH48	ctd micaschist	N44° 55' 27.45'' E7° 08' 16.40''	mu 35%, chl 15%, gph 15%, ctd 15%, q 10%, ilm 10%, ab <5%, pl <5%	22	0.16-0.55	491	27	11
	CH197	ctd micaschist	N44° 55' 42.43'' E7° 11' 9.39''	wm 30%, q 25%, ctd 20%, chl 15%, ilm 5%, gph <5%, g <5%, ab <5%, tur<5%	21	0.20-0.33	532	14	6
	CH11**	g-ctd micaschist	N44° 59' 21.75'' E7° 06' 29.03''	wm 30%, q 30%, ctd 25%, g 5%, chl 5%, gph 5, ep < 5%, ab < 5%, ru < 5%, ilm <5%	19	0.25-0.40	483	17	5
Muret	MU6	ab micaschist	N44° 56' 16.11'' E7° 07' 35.59''	q 25%, wm 25%, ab 20%, chl 15%, g 10%, ilm 5%, gph <5%, tur <5%	24	0.11-0.45	551	21	9
	MU10	g micaschist	N44° 55' 33.46'' E7° 06' 53.74''	q 35%, wm 30%, g 15%, chl 10%, bi 5%, ab 5%, gph <5%	23	0.15-0.45	526	28	12
	MU8	ab micaschist	N44° 56' 28.54'' E7° 06' 11.40''	q 25%, wm 25%, ab 20%, chl 10%, g 5%, ilm 5%, gph 5%, bi 5%	21	0.15-0.45	531	25	11
	MU2110*	g-gl micaschist	N44° 57' 01.29'' E7° 05' 05.84''	wm 30%, q 25%, g 20%, ctd 15%, chl 10%, ilm <5%, ru <5%, gph <5%	22	0.11-0.29	547	22	9
	MU7*	g-ctd micaschist	N44° 56' 05.10'' E7° 04' 10.18''	q 30%, wm 30%, ctd 20%, g 10%, chl 5%, ru < 5%, ilm <5%, gph < 5%	23	0.20-0.38	516	22	9
Serre	SE4	calcschist	44°58'20.56"N 7° 5'13.12"E	cc 50%, q 20%, wm 15% chl 10%, ab <5%, gph 5%, ilm <5%	15	0.32-0.55	480	17	8
	SE16	marble	44°59'6.27"N 7° 5'33.09"E	cc 60%, wm 10%, q 10%, chl 10%, ilm 5%, gph <5%, ab <5%	21	0.12-0.39	513	16	7
	SE2004	calcschist	44°55'16.88"N 7° 3'30.24"E	cc 70%, q 15%, wm 10%, ab 5%, gph 5%	21	0.28-0.45	492	13	6
	SE8*	g-ctd micaschist	44°58'19.37"N 7° 5'15.95"E	wm 30%, q 35%, ctd 15%, g 10%, chl 5%, ru < 5%, ilm <5%, gph <5%, ab < 5%, ep < 5%	22	0.12-0.46	500	48	20

Table S7 RSCM results (number of Raman spectra, R2 ratio, RSCM temperature, standard deviation, and confidence) from the studied samples. **: samples analysed by Manzotti et al. 2022; *: samples analysed by Manzotti et al. 2015

Section S1

LA-ICP-MS chemical mapping

Major element maps of garnet were acquired by LA-ICP-MS with a Resonetics RESOlutionSE 193nm excimer laser system equipped with a S-155 large volume constant geometry cell (Laurin Technic, Australia) at the Institute of Geological Sciences, University of Bern, Switzerland. The laser system was coupled to an Agilent 7900 quadrupole ICP-MS instrument. The ICP-MS was tuned for low oxide production (ThO/Th < 0.2%) and Th/U ratio close to one (Th/U > 97%). Mapping was performed on a regular 30 μm-thick polished thin section. Maps were acquired with 4 μm large parallel rasters and spacing, and a scan speed of 4 μm s^{-1}. Pre-ablation of each raster was performed for minimizing the effect of re-deposition. Ablation was performed in an atmosphere of pure He (0.7 L min^{-1}) and N_2 (0.003 L min^{-1}) mixed with Ar (0.86 L min^{-1}) immediately after the ablation cell. A laser repetition rate of 10 Hz (Fig. 7f), and fluence on sample of 7 J cm^{-2} were employed. Data acquisition was performed in time-resolved analysis mode as a single continuous experiment. Background (30 s) was measured before each scan. Standard glasses GSD-1g and SRM-NIST 612 were analyzed every 30 minutes. Each analysis comprised a series of 25 elements for a total sweep time of 0.39 and 0.41 s.

Data reduction was performed using the software XMapTools (Lanari and Piccoli, 2020; Markmann et al., 2024). Instrument drift and mass bias were corrected for applying a polynomial between the dataset of standards; background was also subtracted from each raster. For garnet, quantification was performed using ^{29}Si for internal calibration based on weighted average of EPMA wt%.

Sample	Mineral	Spot size [um]	Cleaning spot size [um]	Scan speed [um s^{-1}]	Repetition rate [Hz]	Fluence [J cm^{-2}]	Primary standard	Secondary standard
Pi15 ab micaschist	garnet	5	7	4	10	7	GSD-1g	NIST612

Section S2

Raman spectroscopy on carbonaceous material (RSCM) method

Regional metamorphic processes produce a gradual transformation of the organic matter present in rocks to CM (carbonaceous material). The *T* of regional metamorphism controls the degree of graphitization (Beyssac et al. 2002, 2003). Because graphitization is considered as an irreversible process, the *T* estimates are not affected by metamorphic reactions associated with retrogression. Thus, this graphitization process allows us to estimate the peak *T* reached by CM-bearing samples.

Carbonaceous material was analysed in fifteen samples. Raman spectra of CM were obtained at the Laboratoire Magmas et Volcans (Clermont-Ferrand, France) using a Renishaw inVia confocal micro-spectrometer, equipped with a 532 nm diode-pulsed solid state laser. Because RSCM can be affected by several analytical mismatches, we followed closely the analytical procedures described by Beyssac et al. (2002, 2003). Measurements were carried out on polished thin sections using a grating of 2400 grooves/mm, a 20 µm slit aperture (high confocality setting), a ×100 microscope objective, and 1-5 mW laser power on the sample surface. The laser was generally focused at 5-15 µm depth to analyse graphite that was located below different minerals and not exposed at the surface. Each analysis consisted of 6 or 10 accumulations of 20 seconds each in the ~900-2000 cm^{-1} wavenumber range, containing the two principal vibrations of graphite. On each sample, we measured more than 20 different grains of graphite. The spectra were processed using the WiRE™ 4.4 software: first, they were truncated, then a linear baseline correction was applied in the 1200-1800 cm^{-1} spectral range, and finally curve fitting was performed. Three bands (corresponding to G, D1, and D2 components, respectively at ~1580, ~1350, and ~1620 cm^{-1}) were necessary to fit the graphite spectrum. The degree of organization of CM is quantified by the relative area of the G, D1, and D2 components in the Raman spectrum of CM, and expressed as an R2 ratio equal to $D1/(G + D1 + D2)$ (Beyssac et al. 2002, 2003).

Section S3

Garnet fractionation

Very high-resolution plane-polarised photomicrographs of the entire thin sections have been acquired with a Nikon Super Coolscan 9000 ED (Stockholm University). The modal amount of garnet was estimated in each thin section, measuring the garnet surface with respect to the surface of the entire thin section using a graphic software (ImageJ open-source; Rasband, 1997). The proportion of garnet cores has been estimated by image analysis on the basis of backscattered images and X-ray maps using the software ImageJ. X-ray maps were acquired on selected garnet porphyroblasts. Representative chemical compositions of garnet cores were subtracted from the measured bulk composition in proportion to the modal amount of the garnet cores. Because there is no evidence that the andradite component is concentrated in the garnet core with respect to the garnet rim the ratio FeO/Fe_2O_3 in the bulk is considered constant.

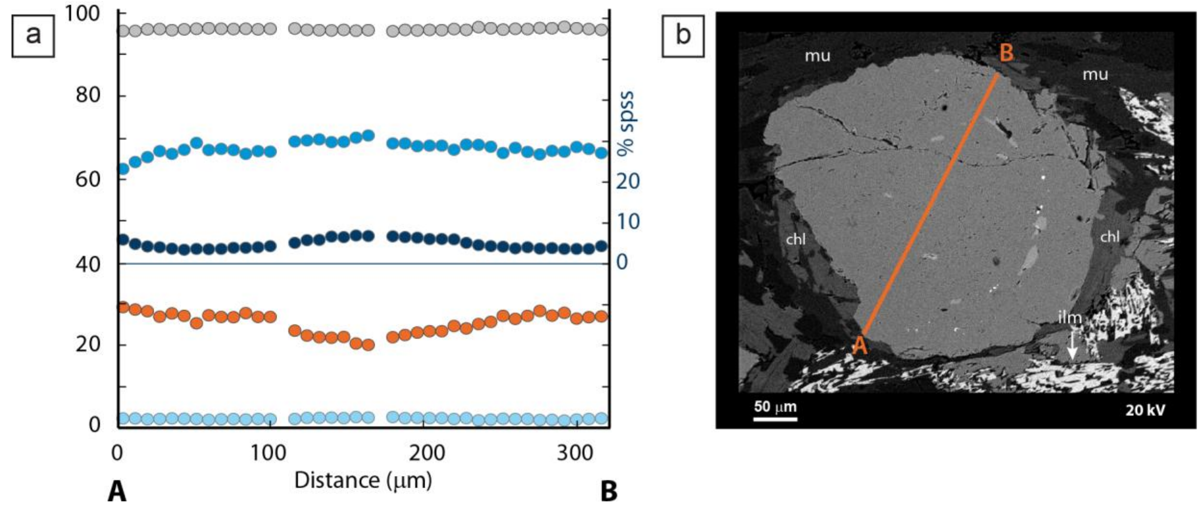

Figure S1 a Garnet compositional profile analysed along the orange line A–B (albite micaschist, sample Pi15). Backscattered image of the analysed garnet. Garnet is wrapped by muscovite and partially replaced by chlorite

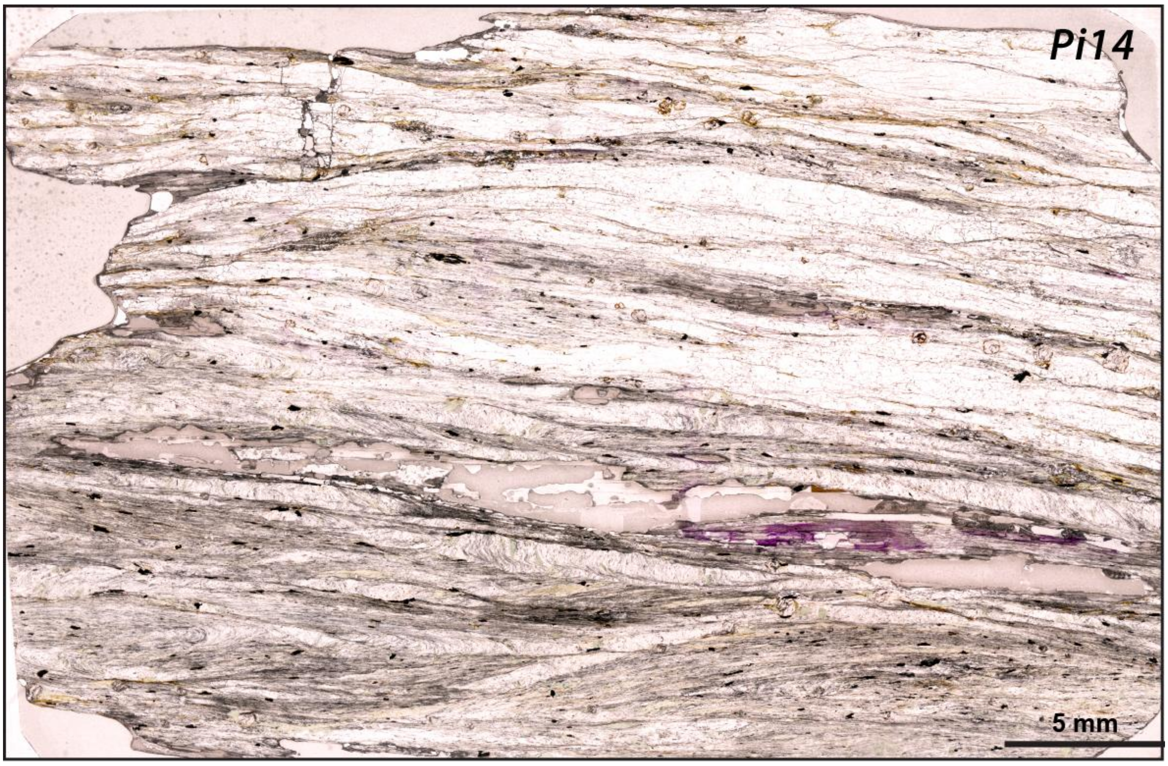

Figure S2 Photomicrograph (plane-polarised) of the chlorite-rich schist sample Pi14 collected south of the Punta Ceresa (section A)

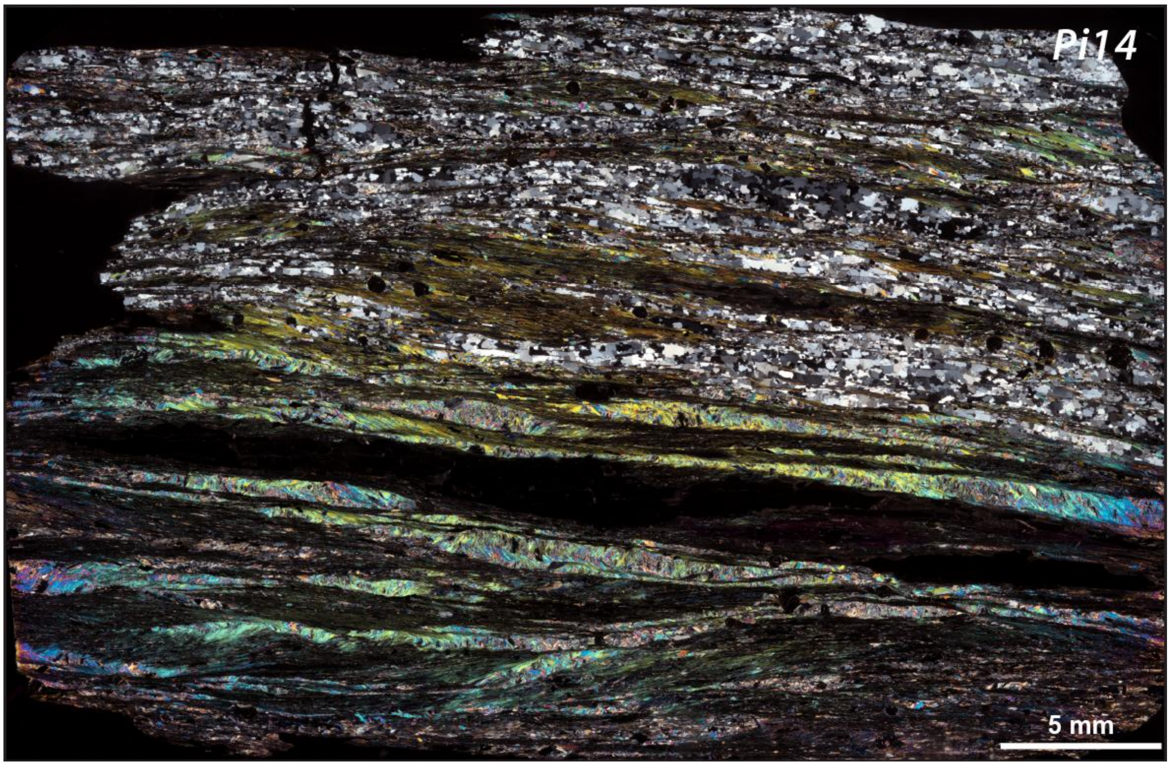

Figure S3 Photomicrograph (cross-polarised light) of the chlorite-rich schist sample Pi14 collected south of the Punta Ceresa (section A)

Figure S4 Photomicrograph (plane-polarised) of the chlorite-rich schist sample Pi14 collected south of the Punta Ceresa (section B)

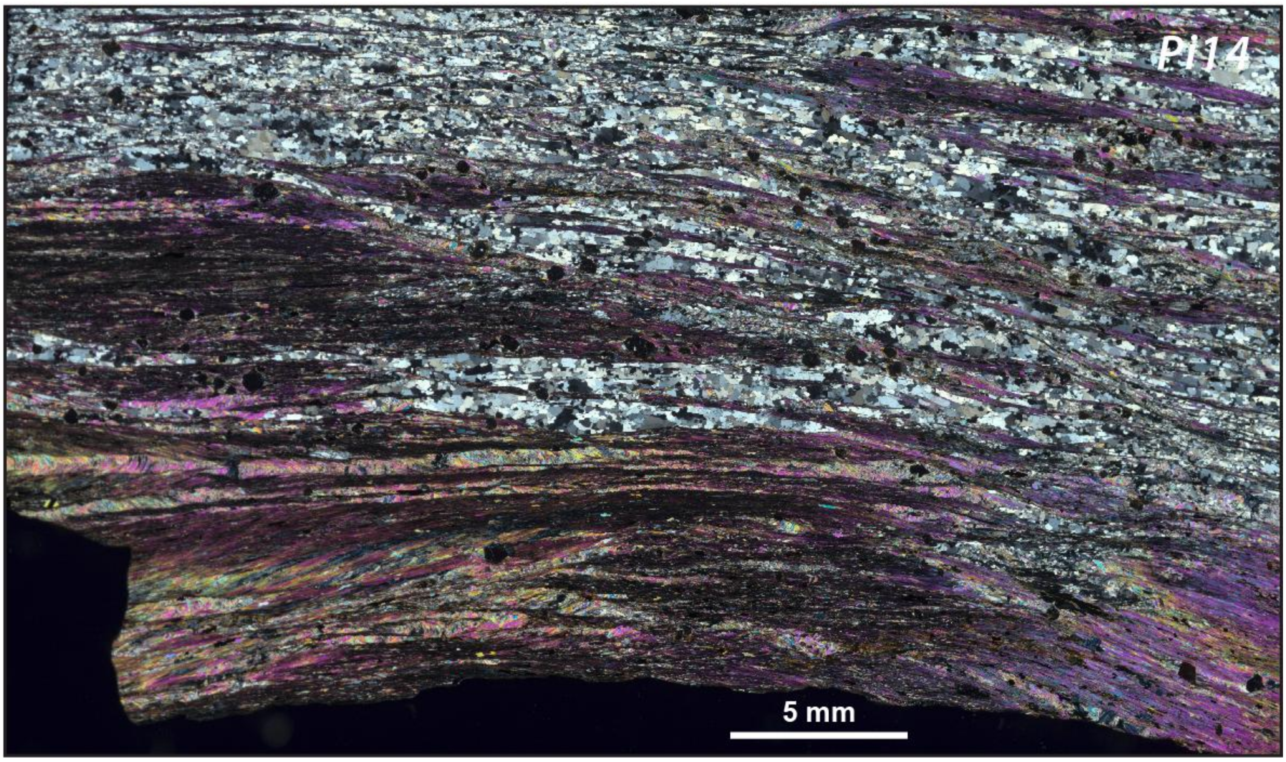

Figure S5 Photomicrograph (cross-polarised light) of the chlorite-rich schist sample Pi14 collected south of the Punta Ceresa (section B)

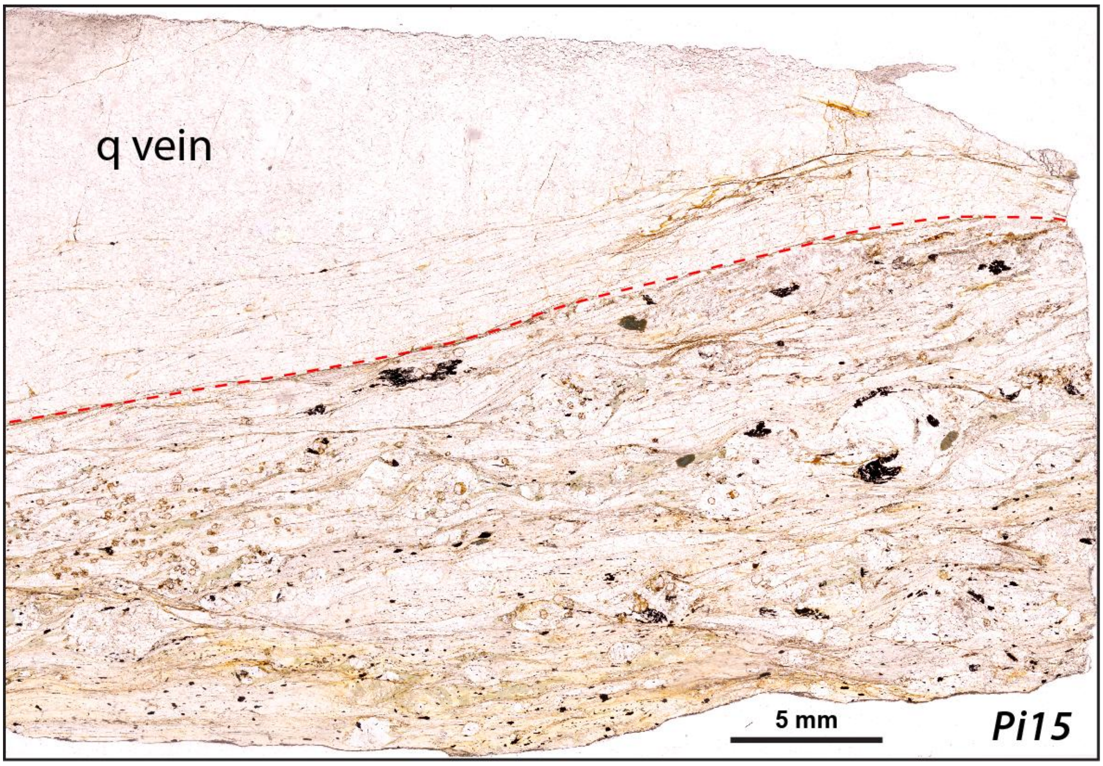

Figure S6 Photomicrograph (plane-polarised) of the albite micaschist sample Pi15 collected close to Bocchiardo

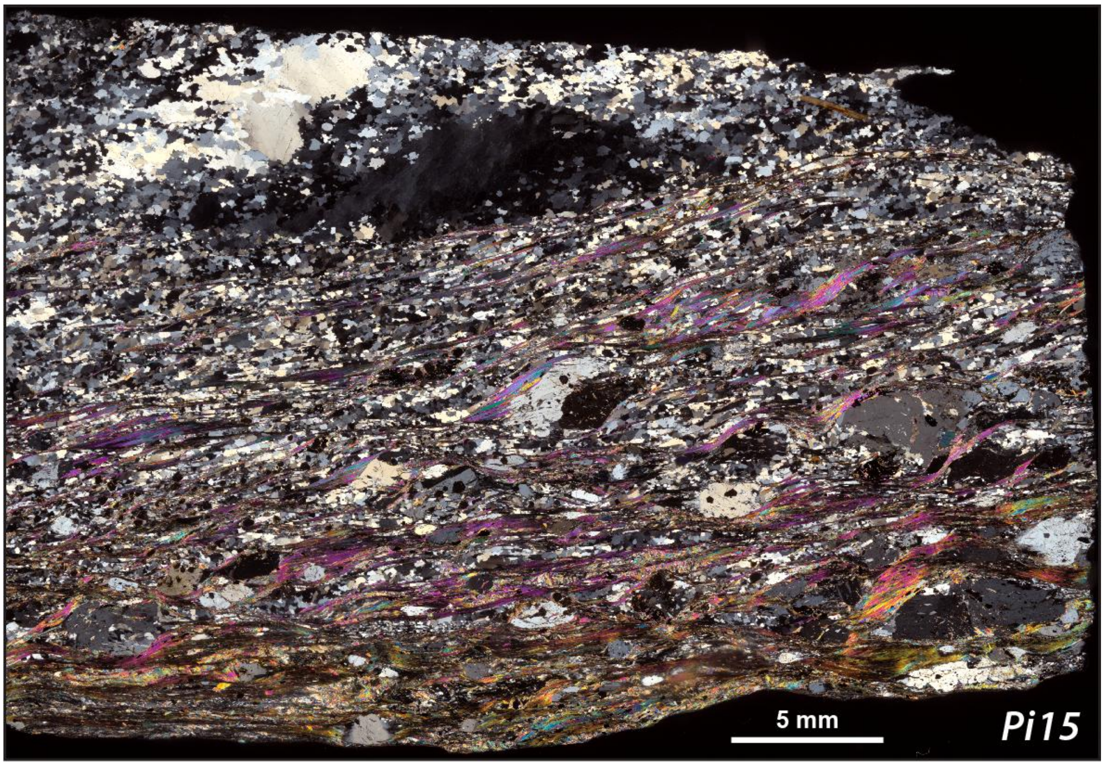

Figure S7 Photomicrograph (cross-polarised light) of the albite micaschist sample Pi15 collected close to Bocchiardo

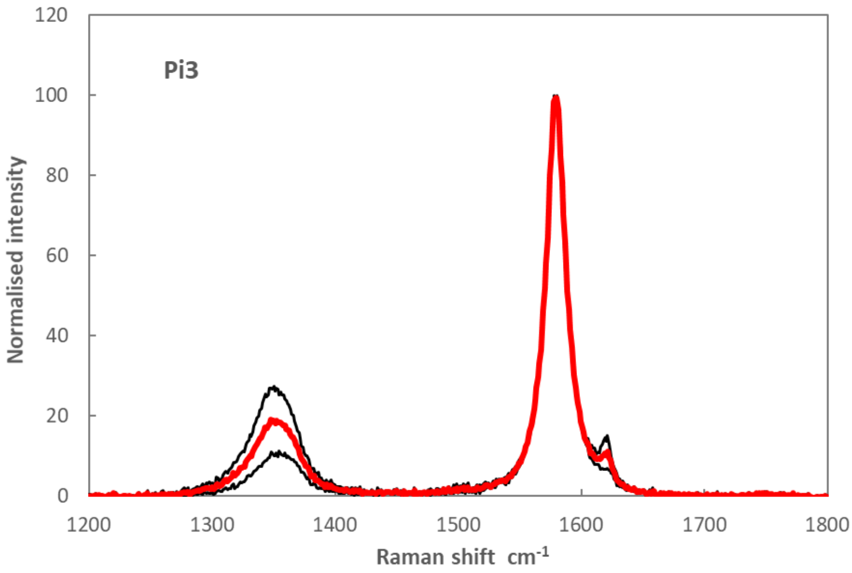
Pi3
Normalised intensity
Raman shift cm-1
0
20
40
60
80
100
120
1200
1300
1400
1500
1600
1700
1800

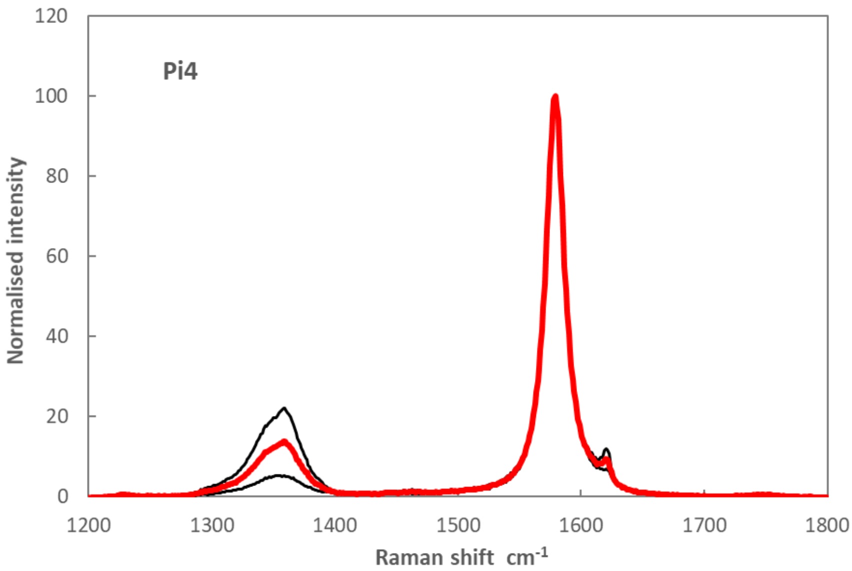
Pi4
Normalised intensity
Raman shift cm-1
0
20
40
60
80
100
120
1200
1300
1400
1500
1600
1700
1800

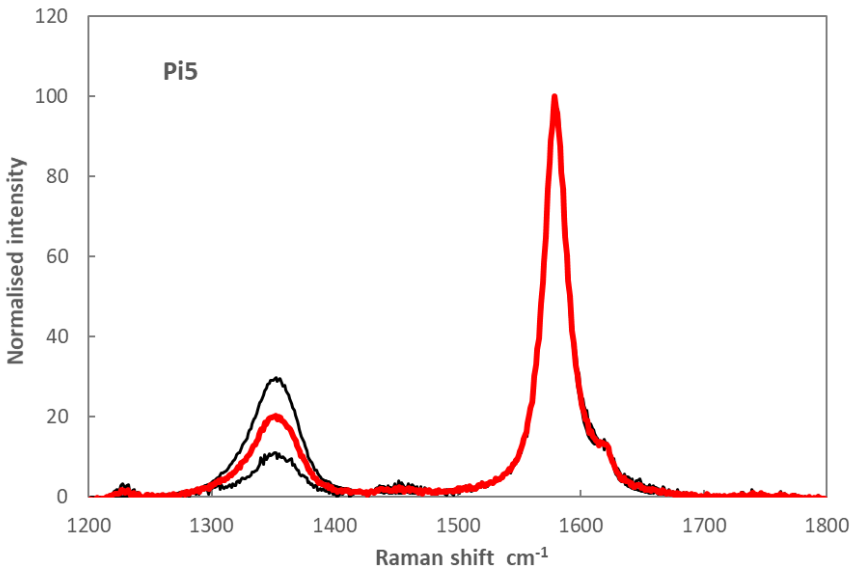
Pi5
Normalised intensity
Raman shift cm-1
0
20
40
60
80
100
120
1200
1300
1400
1500
1600
1700
1800

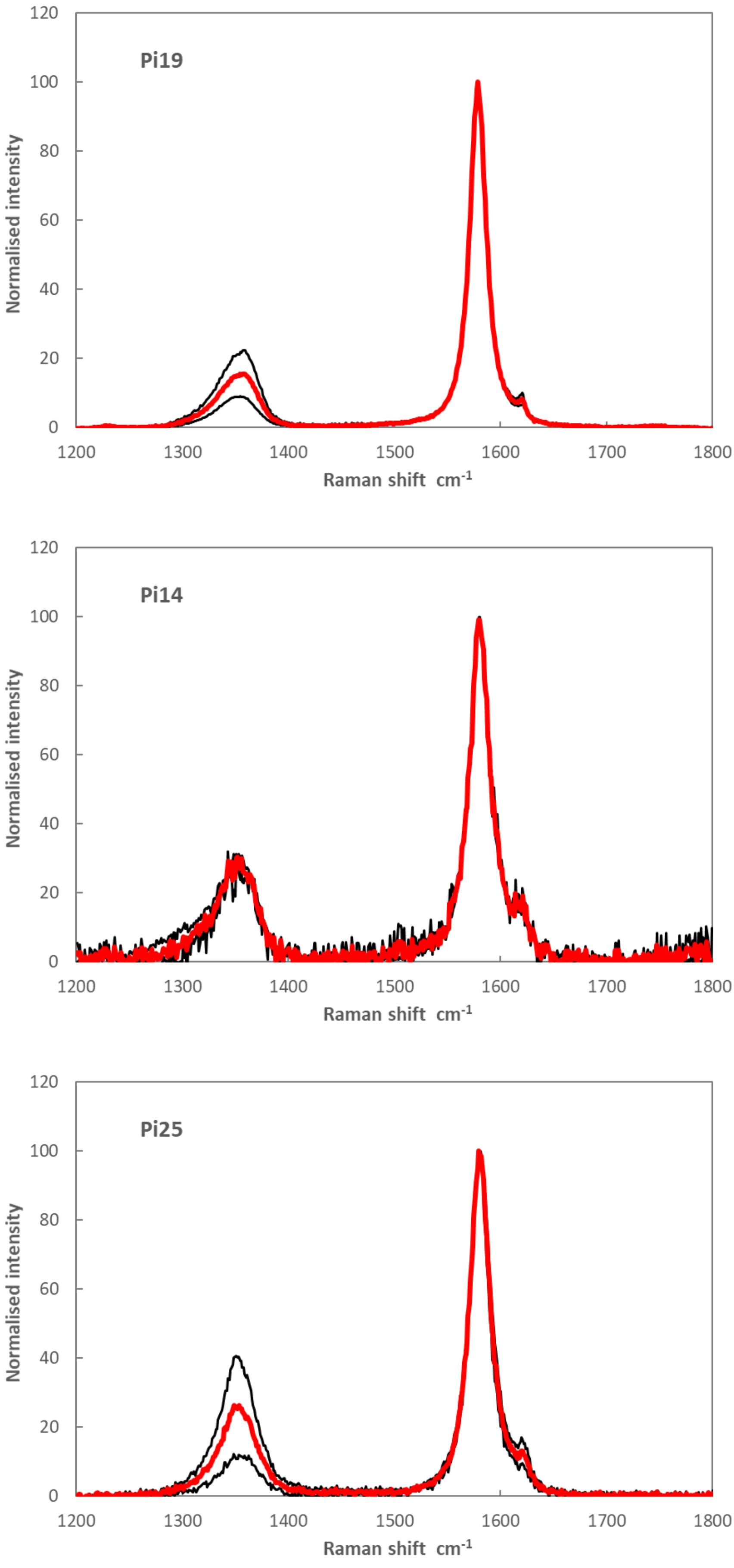
Pi19
Pi14
Pi25
Normalised intensity
Raman shift cm-1
0
20
40
60
80
100
120
1200
1300
1400
1500
1600
1700
1800

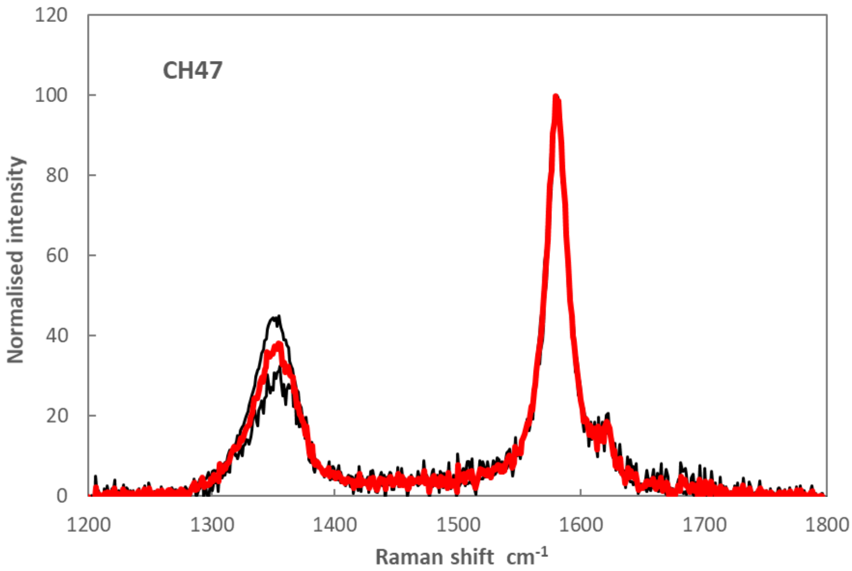
CH47
Normalised intensity
Raman shift cm-1
0
20
40
60
80
100
120
1200
1300
1400
1500
1600
1700
1800

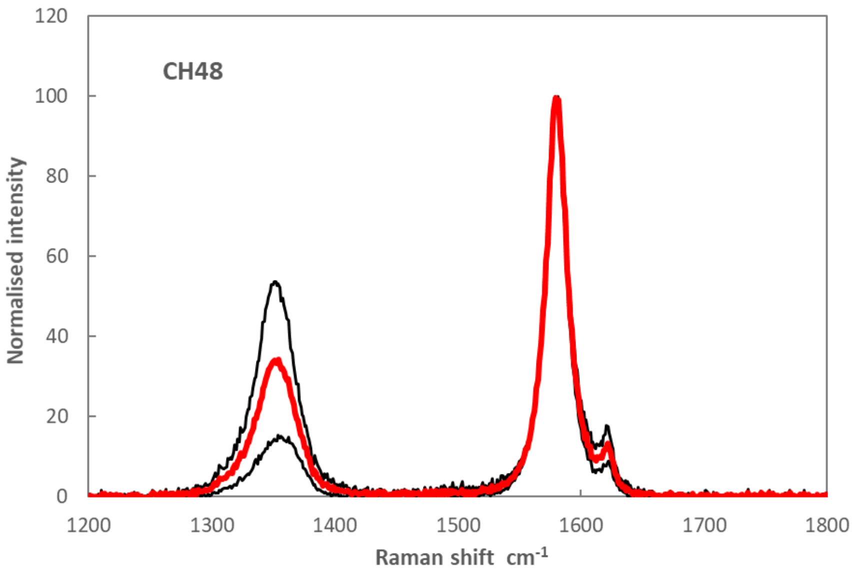
CH48
Normalised intensity
Raman shift cm-1
0
20
40
60
80
100
120
1200
1300
1400
1500
1600
1700
1800

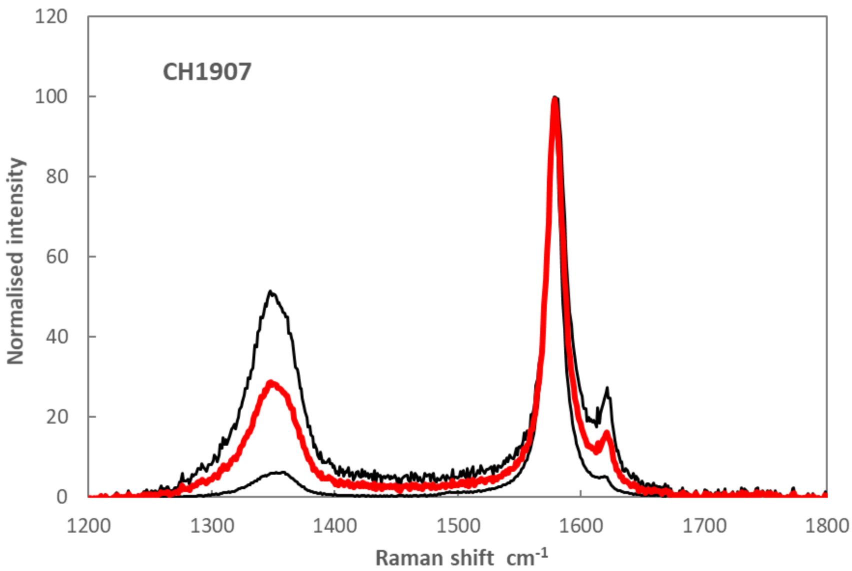
CH1907
Normalised intensity
Raman shift cm-1
0
20
40
60
80
100
120
1200
1300
1400
1500
1600
1700
1800

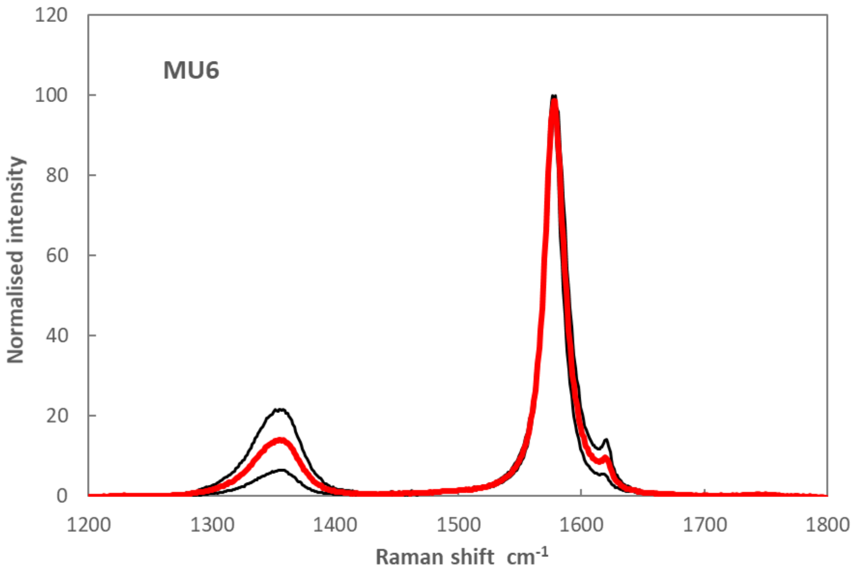
MU6
Normalised intensity
Raman shift cm^{-1}
0
20
40
60
80
100
120
1200
1300
1400
1500
1600
1700
1800

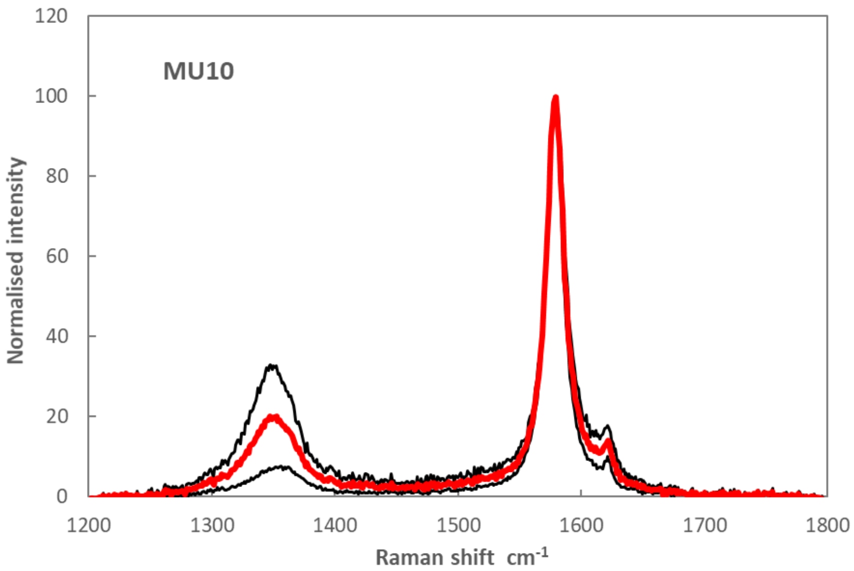
MU10
Normalised intensity
Raman shift cm^{-1}
0
20
40
60
80
100
120
1200
1300
1400
1500
1600
1700
1800

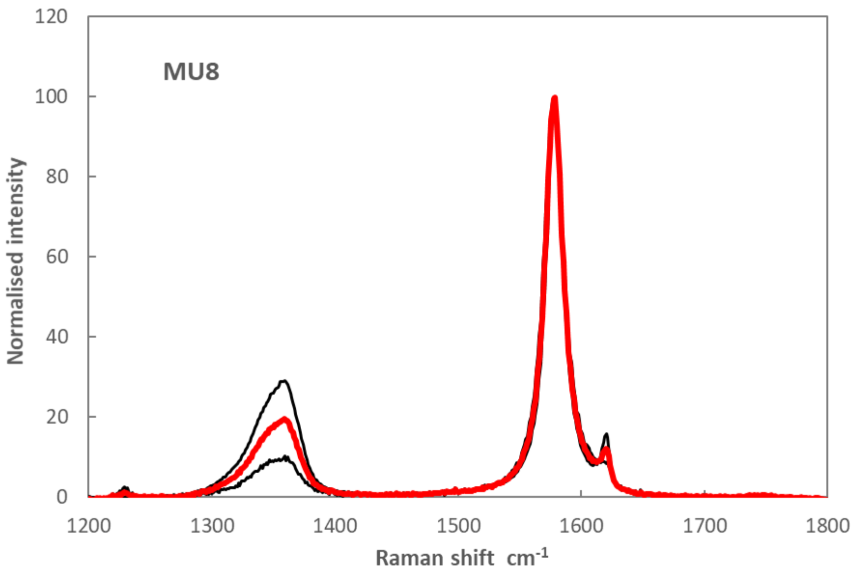
MU8
Normalised intensity
Raman shift cm^{-1}
0
20
40
60
80
100
120
1200
1300
1400
1500
1600
1700
1800

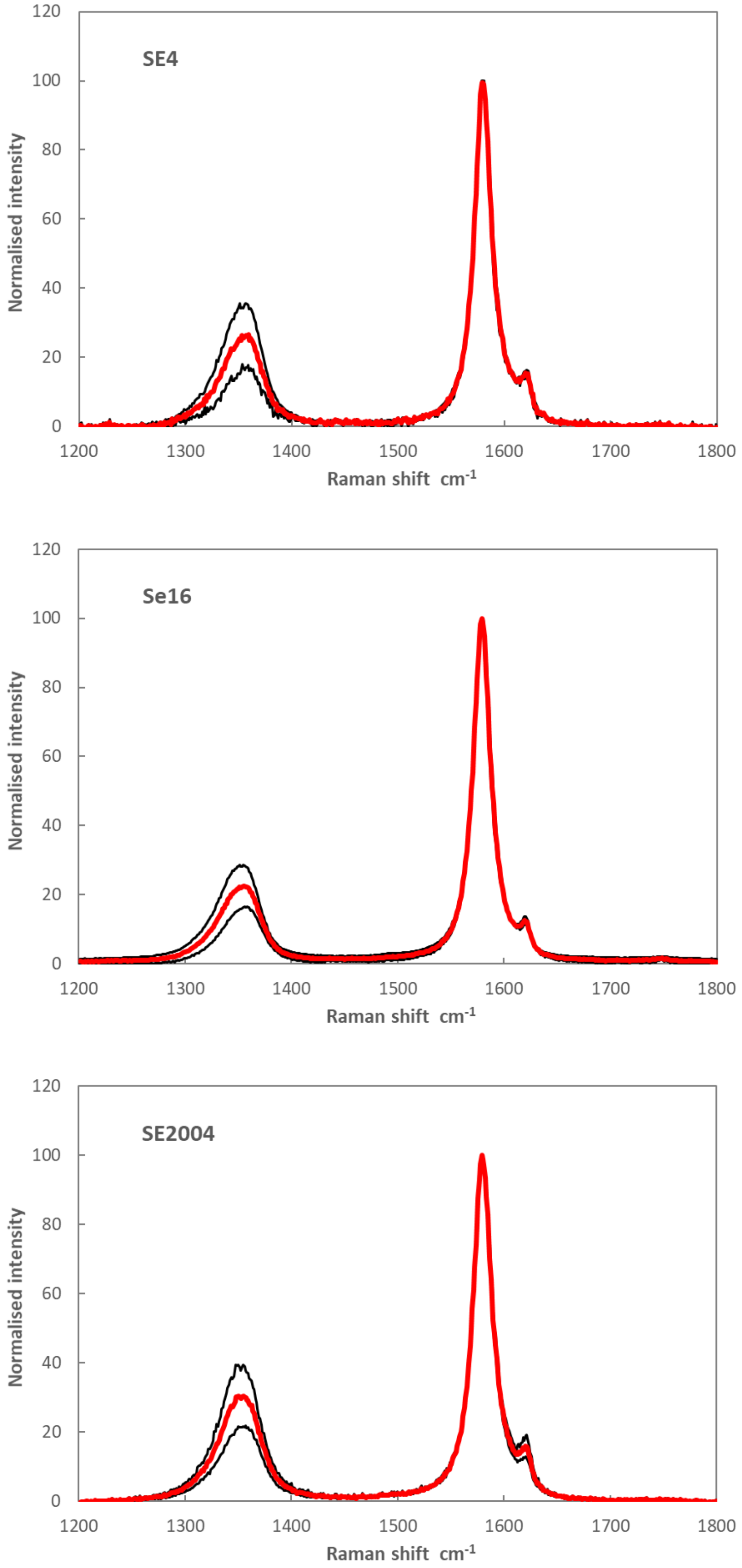

Figure S8 Representative Raman spectra of carbonaceous material from the fifteen analysed samples. For each sample, the spectra corresponding to the maximum, minimum and intermediate temperatures are shown

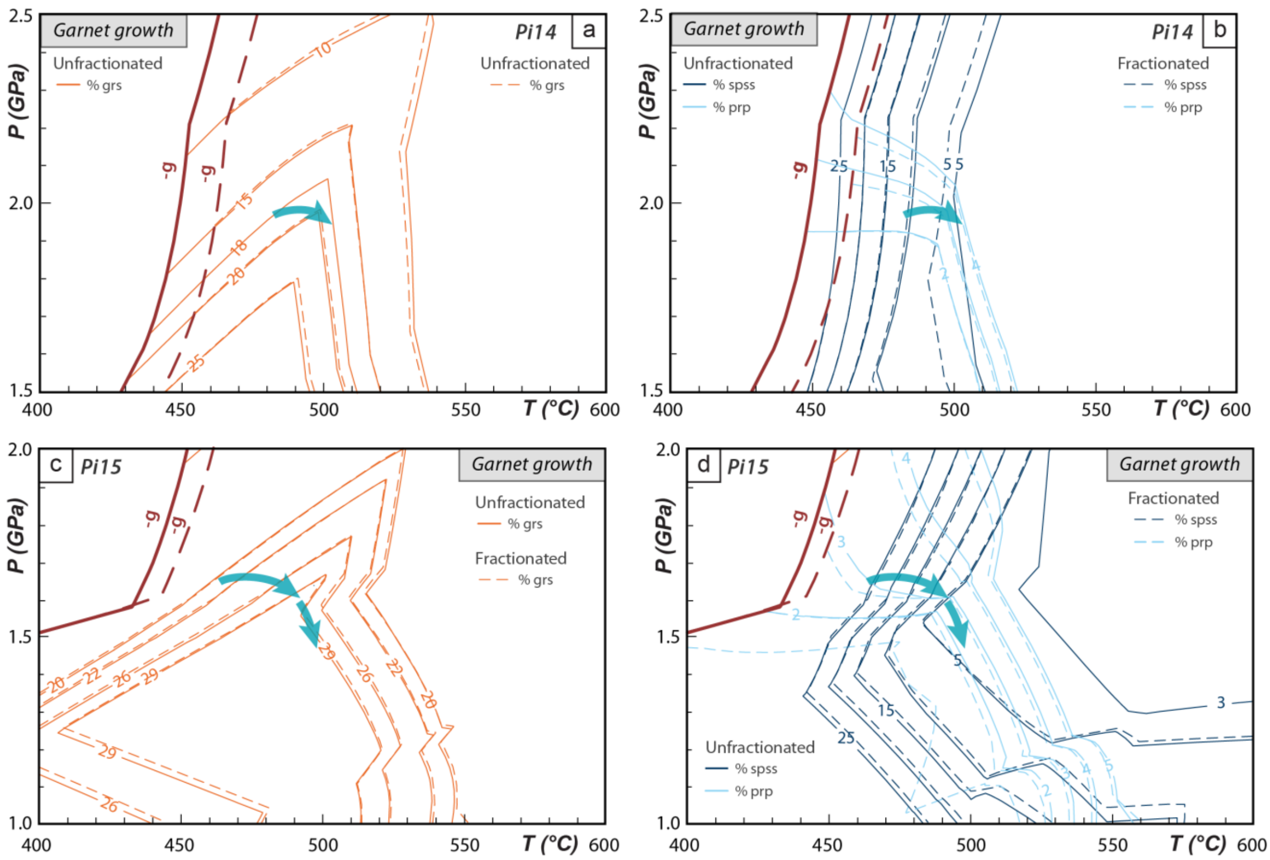

Figure S9 Chemical isopleths for garnet from the chlorite-rich schist Pi14 and albite micaschist Pi15, calculated with the unfractionated (solid lines) and fractionated (dashed lines) bulk compositions. The green arrows are the inferred *P*–*T* paths for garnet growth for the two samples

References

Beyssac O, Goffé B, Chopin C, Rouzaud JN (2002) Raman spectra of carbonaceous material in metasediments: a new geothermometer. J Metamorph Geol 20:859–871

Beyssac O, Goffé B, Petitet JP, Froigneux E, Moreau M, Rouzaud JN (2003) On the characterization of disordered and heterogeneous carbonaceous materials using Raman spectroscopy. Spectrochim Acta A 59:2267–2276

de Capitani C, Brown TH (1987) The computation of chemical equilibrium in complex systems containing non-ideal solutions. Geochim Cosmochim Acta, 51:2639–2652

de Capitani C, Petrakakis K (2010) The computation of equilibrium assemblage diagrams with Theriak/Domino software. Amer Miner 95:1006–1016

Green ECR, White RW, Diener JFA, Powell R, Holland TJB, Palin RM (2016) Activity–composition relations for the calculation of partial melting equilibria in metabasic rocks. J Metamorph Geol, 34, 845–869

Holland, TJB, Powell, R (1998) An internally consistent thermodynamic data set for phases of petrological interest. J Metamorph Geol 16:309–343

Holland, TJB, Powell, R (2011) An improved and extended internally consistent thermodynamic dataset for phases of petrological interest, involving a new equation of state for solids. J Metamorph Geol 29:333–383

Holland TJB, Green ECR, Powell R (2022) A thermodynamic model for feldspars in $KAlSi_3O_8$–$NaAlSi_3O_8$–$CaAl_2Si_2O_8$ for mineral equilibrium calculations. J Metamorph Geol 40:587–600

Lanari P, Piccoli F (2020) New horizons in quantitative compositional mapping – Analytical conditions and data reduction using XMAPTOOLS. IOP Conference Series: Materials Science and Engineering 891: 012016

Manzotti P, Schiavi F, Nosenzo F, Pitra P, Ballèvre M (2022) A journey towards the forbidden zone: a new, cold, UHP unit in the Dora-Maira Massif (Western Alps). Contrib Mineral Petrol 177:59

Manzotti P, Schiavi F, Ballèvre M, Nosenzo F (2025) Garnet growth across the quartz-coesite transition in metapelites: equilibrium vs. kinetics. Eur J Mineral 37:455–482

Markmann TA, Lanari P, Piccoli F, Pettke T, Tamblyn R, Tedeschi M, Lueder M, Kunz BE, Riel N, Laughton J (2024) Multi-phase quantitative compositional mapping by LA-ICP-MS: Analytical approach and data reduction protocol implemented in XMapTools. Chem Geol 646:121895

Pouchou JL, Pichoir F (1985) “PAP” $\phi(\rho Z)$ procedure for improved quantitative microanalysis. In: Armstrong JT (ed) Microbeam Analysis. San Francisco Press, San Francisco, CA, pp 104–106

Powell R, White RW, Green ECR, Holland TJB, Diener JFA (2014). On parameterising thermodynamic descriptions of minerals for petrological calculations. J Metamorph Geol 32:245–260

Rasband W (1997) ImageJ. In: U.S. National Institutes of Health. U.S. National Institutes of Health http://imageJ.nih.gov

White RW, Powell R, Johnson TE (2014a) The effect of Mn on mineral stability in metapelites revisited: new a–x relations for manganese-bearing minerals. J Metamorph Geol 32:809–828

White RW, Powell R, Holland TJB, Johnson TE, Green ECR (2014b) New mineral activity–composition relations for thermodynamic calculations in metapelitic systems. J Metamorph Geol 32:261–286